

# Search for Majoron-emitting modes of double-beta decay of $^{136}\text{Xe}$ with EXO-200

J. B. Albert,<sup>1</sup> D. J. Auty,<sup>2</sup> P. S. Barbeau,<sup>3</sup> E. Beauchamp,<sup>4</sup> D. Beck,<sup>5</sup> V. Belov,<sup>6</sup> C. Benitez-Medina,<sup>7,\*</sup> M. Breidenbach,<sup>8</sup> T. Brunner,<sup>9</sup> A. Burenkov,<sup>6</sup> G. F. Cao,<sup>10</sup> C. Chambers,<sup>7</sup> J. Chaves,<sup>9</sup> B. Cleveland,<sup>4,†</sup> M. Coon,<sup>5</sup> A. Craycraft,<sup>7</sup> T. Daniels,<sup>11</sup> M. Danilov,<sup>6</sup> S. J. Daugherty,<sup>1</sup> C. G. Davis,<sup>12,‡</sup> J. Davis,<sup>9</sup> R. DeVoe,<sup>9</sup> S. Delaquis,<sup>13</sup> T. Didberidze,<sup>2</sup> A. Dolgolenko,<sup>6</sup> M. J. Dolinski,<sup>14</sup> M. Dunford,<sup>15</sup> W. Fairbank, Jr.,<sup>7</sup> J. Farine,<sup>4</sup> W. Feldmeier,<sup>16</sup> P. Fierlinger,<sup>16</sup> D. Fudenberg,<sup>9</sup> G. Giroux,<sup>13,§</sup> R. Gornea,<sup>13</sup> K. Graham,<sup>15</sup> G. Gratta,<sup>9</sup> C. Hall,<sup>12</sup> S. Herrin,<sup>8</sup> M. Hughes,<sup>2</sup> M. J. Jewell,<sup>9</sup> X. S. Jiang,<sup>10</sup> A. Johnson,<sup>8</sup> T. N. Johnson,<sup>1</sup> S. Johnston,<sup>11</sup> A. Karelin,<sup>6</sup> L. J. Kaufman,<sup>1</sup> R. Killick,<sup>15</sup> T. Koffas,<sup>15</sup> S. Kravitz,<sup>9</sup> A. Kuchenkov,<sup>6</sup> K. S. Kumar,<sup>11</sup> D. S. Leonard,<sup>17</sup> F. Leonard,<sup>15</sup> C. Licciardi,<sup>15</sup> Y. H. Lin,<sup>14</sup> J. Ling,<sup>5</sup> R. MacLellan,<sup>8</sup> M. G. Marino,<sup>16</sup> B. Mong,<sup>4</sup> D. Moore,<sup>9</sup> R. Nelson,<sup>18</sup> A. Odian,<sup>8</sup> I. Ostrovskiy,<sup>9,||</sup> C. Ouellet,<sup>15</sup> A. Piepke,<sup>2</sup> A. Pocar,<sup>11</sup> C. Y. Prescott,<sup>8</sup> A. Rivas,<sup>9</sup> P. C. Rowson,<sup>8</sup> M. P. Roza,<sup>15</sup> J. J. Russell,<sup>8</sup> A. Schubert,<sup>9</sup> D. Sinclair,<sup>15,19</sup> E. Smith,<sup>14</sup> V. Stekhanov,<sup>6</sup> M. Tarka,<sup>5</sup> T. Tolba,<sup>13</sup> D. Tosi,<sup>9,¶</sup> R. Tsang,<sup>2</sup> K. Twelker,<sup>9</sup> P. Vogel,<sup>20</sup> J.-L. Vuilleumier,<sup>13</sup> A. Waite,<sup>8</sup> J. Walton,<sup>5</sup> T. Walton,<sup>7</sup> M. Weber,<sup>9</sup> L. J. Wen,<sup>10</sup> U. Wichoski,<sup>4</sup> L. Yang,<sup>5</sup> Y.-R. Yen,<sup>14</sup> O. Ya. Zeldovich<sup>6</sup>

(EXO-200 Collaboration)

<sup>1</sup>Physics Department and CEEM, Indiana University, Bloomington, Indiana 47405, USA<sup>2</sup>Department of Physics and Astronomy, University of Alabama, Tuscaloosa, Alabama 35487, USA<sup>3</sup>Department of Physics, Duke University, and Triangle Universities Nuclear Laboratory (TUNL), Durham, North Carolina 27708, USA<sup>4</sup>Department of Physics, Laurentian University, Sudbury, Ontario P3E 2C6, Canada<sup>5</sup>Physics Department, University of Illinois, Urbana-Champaign, Illinois 61801, USA<sup>6</sup>Institute for Theoretical and Experimental Physics, Moscow, Russia<sup>7</sup>Physics Department, Colorado State University, Fort Collins, Colorado 80523, USA<sup>8</sup>SLAC National Accelerator Laboratory, Stanford, California 94025, USA<sup>9</sup>Physics Department, Stanford University, Stanford, California 94305, USA<sup>10</sup>Institute of High Energy Physics, Beijing, China<sup>11</sup>Physics Department, University of Massachusetts, Amherst, Massachusetts 01003, USA<sup>12</sup>Physics Department, University of Maryland, College Park, Maryland 20742, USA<sup>13</sup>LHEP, Albert Einstein Center, University of Bern, Bern, Switzerland<sup>14</sup>Department of Physics, Drexel University, Philadelphia, Pennsylvania 19104, USA<sup>15</sup>Physics Department, Carleton University, Ottawa, Ontario K1S 5B6, Canada<sup>16</sup>Technische Universität München, Physikdepartment and Excellence Cluster Universe, Garching, Germany<sup>17</sup>Department of Physics, University of Seoul, Seoul, Korea<sup>18</sup>Waste Isolation Pilot Plant, Carlsbad, New Mexico 88220, USA<sup>19</sup>TRIUMF, Vancouver, British Columbia V6T 2A3, Canada<sup>20</sup>Kellogg Lab, Caltech, Pasadena, California 91125, USA

(Received 24 September 2014; published 10 November 2014)

EXO-200 is a single phase liquid xenon detector designed to search for neutrinoless double-beta decay of  $^{136}\text{Xe}$ . Here, we report on a search for various Majoron-emitting modes based on 100 kg yr exposure of  $^{136}\text{Xe}$ . A lower limit of  $T_{1/2}^{136\text{Xe}} > 1.2 \times 10^{24}$  yr at 90% C.L. on the half-life of the spectral index = 1 Majoron decay was obtained, corresponding to a constraint on the Majoron-neutrino coupling constant of  $|\langle g_{ee}^M \rangle| < (0.8-1.7) \times 10^{-5}$ .

DOI: 10.1103/PhysRevD.90.092004

PACS numbers: 23.40.-s, 14.60.Pq, 14.80.Va, 21.10.Tg

## I. INTRODUCTION

Double-beta decay ( $\beta\beta$ ) is a rare radioactive transition between two nuclei with the same mass number  $A$  and with the nuclear charges  $Z$  different by two units. The process can only proceed when the initial even-even nucleus is less bound than the final one, and can only be observed when both are more bound than the intermediate odd-odd nucleus (or the decay to the intermediate nucleus is highly

\*Present address: Intel, Hillsboro, Oregon, USA.

†Also at SNOLAB, Sudbury, Ontario, Canada.

‡Present address: Naval Research Lab, Washington, D.C., USA.

§Present address: Queen's University, Kingston, Ontario, Canada.

||ostrov@stanford.edu

¶Present address: University of Wisconsin, Madison, Wisconsin, USA.

suppressed, as in  $^{48}\text{Ca}$ ). Thus, in  $\beta\beta$  decay, two neutrons are transformed into two protons and two electrons simultaneously, with or without the emission of additional neutral particles.

Several modes of the  $\beta\beta$  decay are considered in the literature. The mode where two antineutrinos are emitted together with the electrons (the two neutrino decay  $2\nu\beta\beta$ ) is an allowed decay in the standard model that conserves total lepton number. This mode has been observed in several cases, in particular recently in  $^{136}\text{Xe}$  [1,2] with a half-life of  $T^{2\nu\beta\beta} = 2.165 \pm 0.016(\text{stat}) \pm 0.059(\text{sys}) \times 10^{21}$  yr [3]. In contrast, there are alternative, so-far-unobserved, neutrinoless modes where the total lepton number is not conserved and whose existence requires that neutrinos are massive Majorana particles [4]. The simplest of such modes, the  $0\nu\beta\beta$  decay with the emission of two electrons, and nothing else, is a subject of an intense experimental search. In particular, for  $^{136}\text{Xe}$  half-life limits have most recently been set to  $> 1.1 \times 10^{25}$  yr [5] and  $> 1.9 \times 10^{25}$  yr [6].

In this work we derive half-life limits for the neutrinoless modes of  $^{136}\text{Xe}$  in which one or two additional bosons, denoted as  $\chi_0$  here, are emitted together with the electrons, schematically

$$(A, Z) \rightarrow (A, Z + 2) + 2e^- + \chi_0, \quad (1)$$

or

$$(A, Z) \rightarrow (A, Z + 2) + 2e^- + 2\chi_0. \quad (2)$$

The boson(s) emitted in the  $0\nu\beta\beta\chi_0$  or  $0\nu\beta\beta\chi_0\chi_0$  modes is (are) usually referred to as Majoron(s). Originally described as a Goldstone boson associated with spontaneous lepton number symmetry breaking, Majorons are possible dark matter candidates [7] and may be involved in other cosmological and astrophysical processes (e.g., [8,9]). Although the original proposals by Gelmini and Roncadelli [10] and Georgi *et al.* [11] are disfavored by precise measurement of the width of the Z boson decay to invisible channels [12], other analogous models were proposed, free of this constraint, in which Majoron more generally refers to massless or light bosons that might be neither Goldstone bosons nor required to carry a lepton charge (see [13] and references therein).

The Majoron-emitting modes are experimentally recognizable by the shape of the sum electron spectrum  $S(E_{\text{sum}})$ , characterized by the spectral index  $n$ ,

$$S(E_{\text{sum}}) = \int_1^{E_{\text{sum}}-1} F(Z, E_1) E_1 p_1 F(Z, E_2) \times E_2 p_2 (E_{\text{tot}} - E_1 - E_2)^n dE_1 dE_2 \times \delta(E_{\text{sum}} - E_1 - E_2), \quad (3)$$

where  $E_1$ ,  $p_1$ ,  $E_2$ , and  $p_2$  are the energy and momentum for each of the two electrons and  $E_{\text{sum}} = E_1 + E_2$  is the

observable sum energy,  $E_{\text{tot}}$  is the total available energy, i.e., the decay Q value plus two electron masses, and the spectral index is an integer  $n = 1, 2, 3$ , or  $7$ .  $F(Z, E)$  is the Fermi function that represents the effect of the nuclear (and atomic) Coulomb field on the wave function of the outgoing electron. All energies are in units of the electron mass  $m_e$  and thus the function  $S(E_{\text{sum}})$  is dimensionless. Note that  $n=5$  for the observed  $2\nu\beta\beta$  decay. The normalized spectra for  $^{136}\text{Xe}$  and various spectral indices are illustrated in Fig. 1.

It is beyond the scope of this paper to discuss the characteristic features of the different Majoron models that are discussed in [14,15]. Generally, the half-life, effective Majoron-neutrino coupling constant  $g_\alpha$ , phase space integral, and the nuclear matrix elements  $M^\alpha$  are related by

$$\frac{1}{T_{1/2}} = |\langle g_\alpha \rangle|^m \cdot |M'^\alpha|^2 \cdot G_\alpha^{0\nu M}(Z, E_0), \quad (4)$$

where  $M'^\alpha = M^\alpha \left(\frac{g_A}{1.25}\right)^2$ ,  $g_A$  is the axial coupling constant,  $m = 2(4)$  for the emission of one (two) Majorons, and  $G_\alpha^{0\nu M}(Z, E_0)$  is the un-normalized phase space integral that depends on the model type,  $\alpha$  (see Table I), and contains all the necessary fundamental constants. For completeness we show in Table I the most important characteristics of ten Majoron models considered in recent experimental  $\beta\beta$  decay searches [16,17].

Table II shows the phase space integrals for different values of the spectral index for  $^{136}\text{Xe}$ . For numerical calculations it is important to employ accurate values of the Fermi function  $F(Z, E)$ . The  $F(Z, E)$  used in preparing this table was calculated by a code [20] that fully includes the nuclear finite size and electron screening and, as recently recommended [21], evaluates  $F(Z, E)$  at the nuclear radius  $R$ .

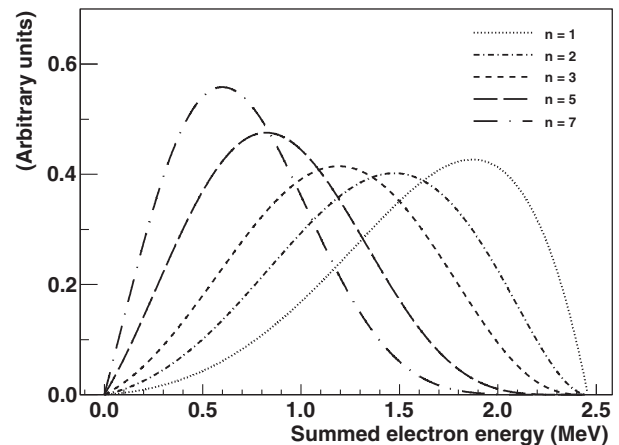


FIG. 1. Spectra for the  $n = 1, 2, 3$ , and  $7$  Majorons, as well as for the  $2\nu\beta\beta$  ( $n = 5$ ) decays of  $^{136}\text{Xe}$ .

TABLE I. Different Majoron-emitting models of  $0\nu\beta\beta$  decay. Class I (II) corresponds to lepton-number-violating (-conserving) models, with subclasses, denoted by letters, corresponding to different quantum numbers of a new particle (detailed description of the classification scheme in [14,15,18]). In the bulk model, built in the context of the brane-bulk scenarios for particle physics, the Majoron is a bulk singlet whose Kaluza-Klein excitations may make it visible in  $0\nu\beta\beta$  decay [19].

Model type, $\alpha$	Number of Majorons emitted in $0\nu\beta\beta$ decay, $m$	The Majoron is a Goldstone boson	Lepton charge, $L$	Spectral index, $n$
IB	1	no	0	1
IC	1	yes	0	1
ID	2	no	0	3
IE	2	yes	0	3
IIB	1	no	-2	1
IIC	1	yes	-2	3
IID	2	no	-1	3
III	2	no	-1	7
IIIF	1	no	-2	3
“Bulk”	1	no	0	2

## II. DETECTOR DESCRIPTION

The EXO-200 detector is a cylindrical single phase time projection chamber (TPC) filled with liquid xenon enriched to 80.6% in  $^{136}\text{Xe}$ . A detailed description of the detector is available elsewhere [22]. The detector is constructed from components carefully selected to minimize internal radioactivity [23]. External radioactivity is shielded by 25 cm thick lead walls surrounding the detector on all sides. Additional passive shielding is provided by  $\sim 50$  cm of high purity cryogenic fluid [24] filling the copper cryostat with a wall thickness of 5.4 cm that houses the TPC. The detector is located inside a clean room at the Waste Isolation Pilot Plant (WIPP) in Carlsbad, New Mexico, USA, under an overburden of  $1585_{-6}^{+11}$  meters water equivalent [25]. The remaining cosmic ray flux is detected by an active muon veto system consisting of plastic scintillation panels surrounding the clean room on four sides. Energy deposited in the TPC by ionizing radiation produces free charge and scintillation light, which are registered by anode wire grids and arrays of avalanche photodiodes, respectively. The TPC allows for three-dimensional position reconstruction of energy depositions, providing further discrimination

against gamma backgrounds. Charge deposits (clusters) in a given event that are spatially separated by  $\sim 1$  cm or more can be individually resolved. The event can then be classified as single site (SS), or multisite (MS), depending on the number of observed charge clusters. Based on Monte Carlo (MC) simulation,  $>90\%$  of  $\beta\beta$  events are expected to be reconstructed as SS, while the energy-averaged fraction of SS gamma events is around 30%. Total energy of an event is determined by combining the charge and scintillation signals, which achieves better energy resolution than in each individual channel due to the anticorrelation between them [26]. Radioactive gamma sources are periodically deployed at several positions near the TPC to characterize the detector response and validate the MC simulation.

## III. EXPERIMENTAL DATA AND ANALYSIS

The data set and event selection criteria used in this work are the same as in the recent search for the neutrino mediated  $0\nu\beta\beta$  decay [5]. The data were collected between September 22, 2011, and September 1, 2013, resulting in the total of  $477.60 \pm 0.01$  live days. The fiducial volume is described by a hexagon with an apothem of 162 mm and absolute length coordinate values between 10 and 182 mm (with  $Z = 0$  corresponding to the cathode location). This translates into a  $^{136}\text{Xe}$  mass of 76.5 kg, or  $3.39 \times 10^{26}$  atoms of  $^{136}\text{Xe}$ , and an exposure of 100 kg yr (736 mol yr).

The calibrated energy  $E$  is obtained as  $E = p_0 + p_1 E_r + p_2 E_r^2$ , where  $E_r$  is the measured energy and  $p_0$ ,  $p_1$ , and  $p_2$  are empirical constants. The measured energy is assumed to follow a conditional Gaussian distribution, with the following energy-dependent resolution:  $\sigma^2(E) = \sigma_{\text{elec}}^2 + bE + cE^2$ , where  $\sigma_{\text{elec}}$  is interpreted as the electronic noise contribution,  $bE$  represents statistical fluctuations in the ionization and scintillation, and  $cE^2$  is assumed to be a position- and time-dependent broadening. In this analysis, both the energy scale and resolution are determined by fitting the full shape of true energy spectra, as generated by MC, to the corresponding calibration data. This minimizes potential biases caused by determining peak positions and widths using simplified analytical fit models. It allows one to constrain the calibration parameters by utilizing all monoenergetic gamma lines simultaneously in the presence of complex backgrounds due to Compton scatters, summation peaks, and passive detector materials. Before the fit, the

TABLE II. Phase space functions in  $\text{yr}^{-1}$  for various Majoron modes and for the  $2\nu\beta\beta$  decay of  $^{136}\text{Xe}$  evaluated at nuclear radius  $R = 1.2A^{1/3}$  fm. The constants in front of the integral are also shown (where  $G_F$  is the Fermi constant and  $\theta_C$  is the Cabibbo angle). The units are such that all energies in the integrals are in units of  $m_e$ .

Decay mode	$0\nu\beta\beta\chi_0$ $n = 1$	$0\nu\beta\beta\chi_0$ $n = 3$	$0\nu\beta\beta\chi_0\chi_0$ $n = 3$	$2\nu\beta\beta$ $n = 5$	$0\nu\beta\beta\chi_0\chi_0$ $n = 7$
Constant	$\frac{(G_F \cos \theta_C g_A)^4 m_e^0 (\hbar c)^2}{128\pi^7 \hbar \log(2) R^2}$	$\frac{(G_F \cos \theta_C g_A)^4 m_e^0}{32\pi^7 \hbar \log(2)}$	$\frac{(G_F \cos \theta_C g_A)^4 m_e^7 (\hbar c)^2}{6114\pi^9 \hbar \log(2) R^2}$	$\frac{(G_F \cos \theta_C g_A)^4 m_e^2}{240\pi^7 \hbar \log(2)}$	$\frac{(G_F \cos \theta_C g_A)^4 m_e^7 (\hbar c)^2}{107520\pi^9 \hbar \log(2) R^2}$
$G_\alpha^{0\nu M}$	<b><math>1.11 \times 10^{-15}</math></b>	<b><math>4.02 \times 10^{-18}</math></b>	<b><math>8.32 \times 10^{-18}</math></b>	<b><math>3.86 \times 10^{-18}</math></b>	<b><math>3.44 \times 10^{-17}</math></b>

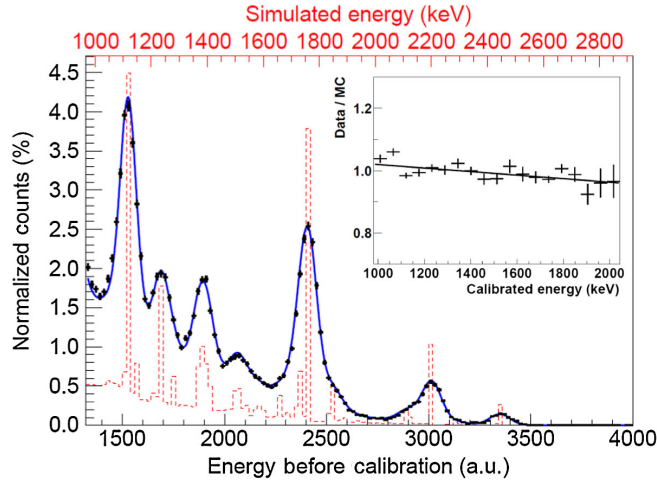


FIG. 2 (color online). Example of an energy spectrum fit using  $^{226}\text{Ra}$  data (black points) and corresponding MC simulation. The dotted line shows the MC energy spectrum before the fit, without the detector effects of energy smearing and at the correct energy scale (indicated by the upper scale in red). The continuous line depicts the resulting MC energy spectrum after the fit to the data points. Only SS events are considered in this example. The data and the smeared MC spectra are each normalized to one. The MC spectrum without energy smearing has an arbitrary normalization. The inset shows the ratio of calibrated data to the smeared MC with the linear fit superimposed (black line).

MC energy spectrum does not include effects of the energy smearing observed with the detector (Fig. 2). In the fitting process, the simulated energy spectra from MC are folded with the measured detector response. The resolution and calibration parameters are fitted simultaneously using a maximum likelihood fit. Similar procedures were used in our previous analyses ([3,5]) to calculate only the resolution parameters. The available source calibration data allow the above fit to be performed on a weekly basis under the assumption of  $c = 0$  and  $p_2 = 0$ . However, comprehensive calibration data acquired less frequently, but with increased statistics, are used to provide a time-averaged quadratic correction to the weekly calibration parameters. This correction is measured at the subpercent level. The correction, as well as the time-averaged resolution parameters used in this analysis, is determined by maximizing a likelihood function that takes into account the live time of physics runs.

Probability density functions (PDFs) for signal and background components are created using a Monte Carlo simulation. Compared to the previous analyses, the MC was improved by substituting simplified modeling of the noise in the signal waveforms with real noise traces sampled from the data and by adjusting the amplitude of simulated signals to better match the data. This resulted in improved agreement between data and MC of the energy threshold for full position reconstruction and improved agreement in average SS fraction. A  $\sim 5\%$  discrepancy in

the shapes of the energy distributions, however, remained. This discrepancy, which is included as a systematic error, manifests itself as an excess of SS events in the data over MC at energies around 1 MeV that gradually and linearly decreases with energy, eventually turning into a deficit (Fig. 2). The PDFs are functions of the two observables: energy and standoff distance (SD). SD is defined as the distance between a charge deposit and the closest material that is not liquid xenon, other than the cathode, emphasizing separation between events originating outside and inside of the chamber. For a multisite event, the smallest standoff distance among multiple charge clusters is used to define SD for the event. Components comprising the overall PDF model are the same as in [5] with the neutrino-mediated  $0\nu\beta\beta$  signal replaced by a Majoron-emitting decay. The parameters of the overall model are the event counts and SS fractions of individual components, and three variables representing normalization terms. The first normalization term is common to all components and is subject to uncertainty due to event reconstruction and selection efficiencies. The second normalization term is specific to the Majoron-emitting decay component and incorporates uncertainty due to discrepancy in shapes of Monte Carlo and data distributions. The third normalization term incorporates uncertainty due to background model incompleteness and applies to background components in the fit. The normalization terms are included in the PDF in a way analogous to the one described in [3].

An important parameter of the PDFs for  $\beta$ -like components [e.g.,  $0\nu\beta\beta\chi_0(\chi_0)$ ] is the  $\beta$  scale, which describes possible difference in energy scales of  $\beta$ -like and  $\gamma$ -like (e.g., external backgrounds) events. The  $\beta$ -scale variable is defined as an energy independent ratio of  $\gamma$  over  $\beta$  energy scales. The  $\beta$  scale is of particular importance for this analysis because adding a  $\beta$ -like component with continuous energy spectrum, such as  $0\nu\beta\beta\chi_0(\chi_0)$ , introduces correlation with the  $2\nu\beta\beta$  component and reduces the accuracy with which both the  $\beta$ -scale and the Majoron components can be determined. While the central values of the  $\beta$  scale found for each mode, as well as for the case of no Majoron mode, are consistent with 1, the corresponding uncertainty increases the final error on each Majoron-emitting decay rate.

A negative log-likelihood function is formed between the data and the overall PDF with the addition of several Gaussian constraints [3] that incorporate systematic uncertainties determined by stand-alone studies. The following parameters are constrained by their corresponding errors, indicated in parentheses: SS fractions (4%), activity of radon in the liquid xenon (10%), common normalization term (8.6%), Majoron-specific normalization term (16% for spectral index  $n = 1$ , 30% for other Majoron modes), background normalization term (20%), and relative fractions of neutron-capture related PDF components (20%). The methodology for determining the systematic errors

follows the one described in [5]. The fit is performed simultaneously for SS and MS events.

#### IV. RESULTS AND CONCLUSION

A profile likelihood scan is performed for each Majoron-emitting  $0\nu\beta\beta$  decay mode separately. The results are consistent with zero amplitude at less than 1 sigma for Majoron-emitting modes with spectral indices 1, 2, and 3, and at  $\sim 2.2$  sigma for  $n = 7$ , as determined with a toy MC study. As a consistency check, we compare the half-life of the  $2\nu\beta\beta$  decay extracted from the fits with additional Majoron components (added one at a time) to the result published previously [3]. The  $2\nu\beta\beta$  half-life values are consistent within 2–3% for the Majoron-emitting decay modes with spectral indices 1, 2, and 3, and within 12% for spectral index 7. Given that the uncertainty on the  $2\nu\beta\beta$  half-life in this measurement reaches  $\sim 8\%$  due to larger fiducial volume and additional correlation with the  $0\nu\beta\beta\chi_0(\chi_0)$  component, we consider these results to be in good agreement. The robustness of the Majoron fits was also checked against the existence of hypothetical backgrounds not included in the background model, in particular  $^{110m}\text{Ag}$  and  $^{88}\text{Y}$ , which have gamma lines with energies close to the maxima of some of the Majoron modes.

Additional fits were performed for each Majoron mode with each background included in the overall model (one at a time). The contribution of these components was found to be effectively constrained by the multisite energy distribution, resulting in much less than 1 sigma impact on the Majoron fits. Figure 3 shows the data set and the best-fit model for the case of the  $n = 1$  Majoron fit. The upper 90% C.L. limits on the number of decays for each of the four Majoron-emitting modes are plotted on the figure all at once, as an illustration.

Table III summarizes the experimental 90% C.L. lower limits on half-lives and upper limits on the effective Majoron-neutrino coupling constants. Equation (4) is used to translate the half-lives into coupling constants, where the phase space factors are taken from Table II, while the matrix elements are taken from [27,28] for the Majoron-emitting decay with  $n = 1$ , and from [15] for other modes. Note that the phase space factor for the  $n = 1$  Majoron is a factor of two larger in [15] than in [29] and [30]. The factor of two is the correct choice, as was acknowledged in [31] and is included in Table II [20].

The spread in the limits on the coupling constants in Table III for a given Majoron mode stems from ambiguity in the matrix elements. The best limits on the coupling constant for the  $n = 1$  Majoron from a laboratory experiment come

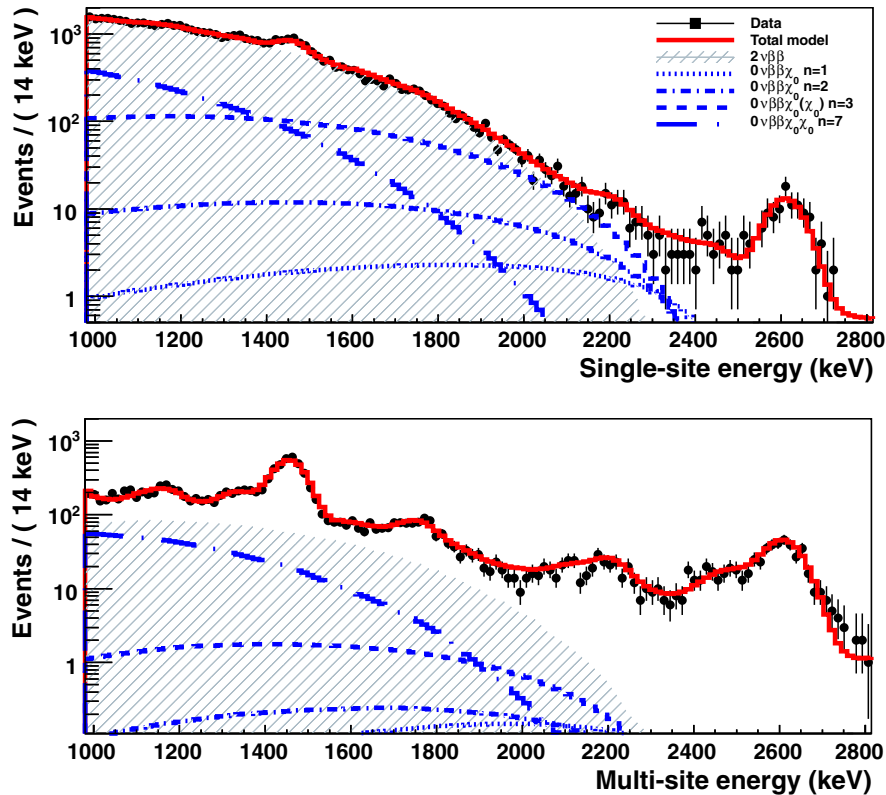


FIG. 3 (color online). SS (top) and MS (bottom) data sets and the best-fit models for the case of the  $n = 1$  Majoron fit. SS energy is predominantly populated by  $\beta$ -like events. The most abundant fit component—the  $2\nu\beta\beta$  decay—is shown in hatched gray. The upper 90% C.L. limits on the number of decays for each of the four Majoron-emitting modes are plotted on the figure all at once, as an illustration.

TABLE III. 90% C.L. limits on half-lives and coupling constants for different Majoron decay models. Spread in coupling constants is due to uncertainty in matrix elements (taken from [27,28] for  $n = 1$  and from [15] for other modes). Phase space factors are taken from Table II.

Decay mode	Spectral index, $n$	Model types	$T_{1/2}$ , yr	$ \langle g_{ee}^M \rangle $
$0\nu\beta\beta\chi_0$	1	IB, IC, IIB	$>1.2 \times 10^{24}$	$<(0.8-1.7) \times 10^{-5}$
$0\nu\beta\beta\chi_0$	2	Bulk	$>2.5 \times 10^{23}$	...
$0\nu\beta\beta\chi_0\chi_0$	3	ID, IE, IID	$>2.7 \times 10^{22}$	$<(0.6-5.5)$
$0\nu\beta\beta\chi_0$	3	IIC, IIF	$>2.7 \times 10^{22}$	$<0.66$
$0\nu\beta\beta\chi_0\chi_0$	7	IIE	$>6.1 \times 10^{21}$	$<(0.5-4.7)$

from NEMO-3 [ $\langle g_{ee}^M \rangle < (1.6-4.2) \times 10^{-5}$ ] [32] and KamLAND-Zen [ $\langle g_{ee}^M \rangle < (0.8-1.6) \times 10^{-5}$ ] [17]. Note that the phase space integral for the  $n = 1$  Majoron used by KamLAND-Zen is about a factor of two smaller than the most up to date value that we used. Therefore, in spite of having a weaker limit on the half-life for the  $n = 1$  Majoron ( $T_{1/2} > 1.2 \times 10^{24}$  yr at 90% C.L.), we report a similar limit on the coupling constant [ $\langle g_{ee}^M \rangle < (0.8-1.7) \times 10^{-5}$ ]. We note that applying the same phase space factor to the KamLAND-Zen's half-life limit would translate it into the limit on the coupling constant of  $\langle g_{ee}^M \rangle < (0.6-1.2) \times 10^{-5}$ .

In conclusion, we report results from a search for Majoron-emitting double-beta decay modes of  $^{136}\text{Xe}$  with two years of EXO-200 data. No statistically significant evidence for this process is found. We obtain limits on the effective coupling constants comparable to the current strongest results by KamLAND-Zen [17] and NEMO-3 [32]. The sensitivity to this and other exotic searches with EXO-200 could be improved in the future with a more precise calibration of the possible difference in  $\beta$  and  $\gamma$  energy scales and the reduction of systematic differences between the spectral shapes in data and MC.

## ACKNOWLEDGMENTS

EXO-200 is supported by DOE and NSF in the United States, NSERC in Canada, SNF in Switzerland, NRF in Korea, RFBR-14-22-03028 in Russia, and DFG Cluster of Excellence ‘‘Universe’’ in Germany. EXO-200 data analysis and simulation uses resources of the National Energy Research Scientific Computing Center (NERSC), which is supported by the Office of Science of the U.S. Department of Energy under Contract No. DE-AC02-05CH11231. The collaboration gratefully acknowledges the WIPP for their hospitality.

- 
- [1] N. Ackerman *et al.* (EXO-200 Collaboration), *Phys. Rev. Lett.* **107**, 212501 (2011).
- [2] A. Gando *et al.* (KamLAND-Zen Collaboration), *Phys. Rev. C* **85**, 045504 (2012).
- [3] J. B. Albert *et al.* (EXO Collaboration), *Phys. Rev. C* **89**, 015502 (2014).
- [4] J. Schechter and J. W. F. Valle, *Phys. Rev. D* **25**, 2951 (1982).
- [5] J. B. Albert *et al.* (EXO-200 Collaboration), *Nature (London)* **510**, 229 (2014).
- [6] A. Gando *et al.* (KamLAND-Zen Collaboration), *Phys. Rev. Lett.* **110**, 062502 (2013).
- [7] M. Lattanzi, S. Riemer-Sørensen, M. Tórtola, and J. W. F. Valle, *Phys. Rev. D* **88**, 063528 (2013).
- [8] A. Dolgov and F. Takahashi, *Nucl. Phys.* **B688**, 189 (2004).
- [9] C. R. Das and J. Pulido, *Phys. Rev. D* **84**, 105040 (2011).
- [10] G. Gelmini and M. Roncandelli, *Phys. Lett.* **99B**, 411 (1981).
- [11] H. Georgi, S. L. Glashow, and S. Nussinov, *Nucl. Phys.* **B193**, 297 (1981).
- [12] The ALEPH Collaboration, The DELPHI Collaboration, The L3 Collaboration, The OPAL Collaboration, The SLD Collaboration, The LEP Electroweak Working Group, The SLD Electroweak, and Heavy Flavour Groups, *Phys. Rep.* **427**, 257 (2006).
- [13] A. Barabash, *Phys. At. Nucl.* **67**, 438 (2004).
- [14] P. Bamert, C. Burgess, and R. Mohapatra, *Nucl. Phys.* **B449**, 25 (1995).
- [15] M. Hirsh, H. Klapdor-Kleingrothaus, S. Kovalenko, and H. Päs, *Phys. Lett. B* **372**, 8 (1996).
- [16] R. Arnold *et al.* (NEMO-3 Collaboration), *Nucl. Phys.* **A765**, 483 (2006).
- [17] A. Gando *et al.* (KamLAND-Zen Collaboration), *Phys. Rev. C* **86**, 021601 (2012).
- [18] C. Burgess and J. Cline, in *Proceedings of the First International Conference on Nonaccelerator Physics, Bangalore, India, 1994*, edited by R. Cowsik (World Scientific, Singapore, 1995).
- [19] R. Mohapatra, A. Peřez-Lorenzana, and C. D. S. Pires, *Phys. Lett. B* **491**, 143 (2000).
- [20] P. Vogel (private communication).
- [21] J. Kotila and F. Iachello, *Phys. Rev. C* **85**, 034316 (2012).
- [22] M. Auger *et al.*, *JINST* **7**, P05010 (2012).
- [23] D. Leonard, P. Grinberg, P. Weber, E. Baussan, Z. Djuricic *et al.*, *Nucl. Instrum. Methods Phys. Res., Sect. A* **591**, 490 (2008).
- [24] 3M HFE-7000, <http://www.3m.com>.
- [25] E. -I. Esch, T. Bowles, A. Hime, A. Pichlmaier, R. Reifarth, and H. Wollnik, *Nucl. Instrum. Methods Phys. Res., Sect. A* **538**, 516 (2005).
- [26] E. Conti, R. DeVoe, G. Gratta, T. Koffas, S. Waldman *et al.*, *Phys. Rev. B* **68**, 054201 (2003).

- [27] J. Menéndez, A. Poves, E. Caurier, and F. Nowacki, *Nucl. Phys. A* **818**, 139 (2009).
- [28] F. Šimkovic, A. Faessler, H. Mütter, V. Rodin, and M. Stauf, *Phys. Rev. C* **79**, 055501 (2009).
- [29] M. Doi, T. Kotani, and E. Takasugi, *Prog. Theor. Phys. Suppl.* **83**, 1 (1985).
- [30] J. Suhonen and O. Civitarese, *Phys. Rep.* **300**, 123 (1998).
- [31] M. Doi, T. Kotani, and E. Takasugi, *Phys. Rev. D* **37**, 2575 (1988).
- [32] R. Arnold *et al.* (NEMO-3 Collaboration), *Phys. Rev. D* **89**, 111101 (2014).